Published in final edited form as:
Nature. 2005 December 8; 438(7069): 820–827. doi:10.1038/nature04186.

VEGFR1-positive haematopoietic bone marrow progenitors initiate the pre-metastatic niche

Rosandra N. Kaplan[1,2,6,*], **Rebecca D. Riba**[1,2,*], **Stergios Zacharoulis**[1,2,6,*], **Anna H. Bramley**[1,2], **Loïc Vincent**[4], **Carla Costa**[1,2], **Daniel D. MacDonald**[1,2], **David K. Jin**[4], **Koji Shido**[4], **Scott A. Kerns**[1,2], **Zhenping Zhu**[8], **Daniel Hicklin**[8], **Yan Wu**[8], **Jeffrey L. Port**[5], **Nasser Altorki**[5], **Elisa R. Port**[7], **Davide Ruggero**[9], **Sergey V. Shmelkov**[1,2,4], **Kristian K. Jensen**[1,2], **Shahin Rafii**[3,4], and **David Lyden**[1,2,6]

[1]Department of Pediatrics and the Children's Blood Foundation Laboratories, Weill Cornell Medical College of Cornell University, 1300 York Avenue, New York, New York 10021, USA.

[2]Department of Cell and Developmental Biology, Weill Cornell Medical College of Cornell University, 1300 York Avenue, New York, New York 10021, USA.

[3]Howard Hughes Medical Institute, Weill Cornell Medical College of Cornell University, 1300 York Avenue, New York, New York 10021, USA.

[4]Department of Genetic Medicine, Weill Cornell Medical College of Cornell University, 1300 York Avenue, New York, New York 10021, USA.

[5]Department of Surgery, Weill Cornell Medical College of Cornell University, 1300 York Avenue, New York, New York 10021, USA.

[6]Department of Pediatrics, Memorial Sloan-Kettering Cancer Center, 1233 York Avenue, New York, New York 10021, USA.

[7]Department of Surgery, Memorial Sloan-Kettering Cancer Center, 1233 York Avenue, New York, New York 10021, USA.

[8]Imclone Systems Incorporated, New York, New York 10014, USA.

[9]Fox Chase Cancer Center, Philadelphia, Pennsylvania 19111, USA.

Abstract

The cellular and molecular mechanisms by which a tumour cell undergoes metastasis to a predetermined location are largely unknown. Here we demonstrate that bone marrow-derived haematopoietic progenitor cells that express vascular endothelial growth factor receptor 1 (VEGFR1; also known as Flt1) home to tumour-specific pre-metastatic sites and form cellular clusters before the arrival of tumour cells. Preventing VEGFR1 function using antibodies or by the removal of VEGFR1$^+$ cells from the bone marrow of wild-type mice abrogates the formation of these pre-metastatic clusters and prevents tumour metastasis, whereas reconstitution with selected Id3 (inhibitor of differentiation 3)-competent VEGFR1$^+$ cells establishes cluster formation and tumour metastasis in Id3 knockout mice. We also show that VEGFR1$^+$ cells express VLA-4 (also known as

Correspondence and requests for materials should be addressed to D.L. (dcl2001@med.cornell.edu) or S.R. (srafii@med.cornell.edu).
*These authors contributed equally to this work.

Supplementary Information is linked to the online version of the paper at www.nature.com/nature.

The authors declare no competing financial interests.

integrin $\alpha_4\beta_1$), and that tumour-specific growth factors upregulate fibronectin—a VLA-4 ligand—in resident fibroblasts, providing a permissive niche for incoming tumour cells. Conditioned media obtained from distinct tumour types with unique patterns of metastatic spread redirected fibronectin expression and cluster formation, thereby transforming the metastatic profile. These findings demonstrate a requirement for VEGFR1$^+$ haematopoietic progenitors in the regulation of metastasis, and suggest that expression patterns of fibronectin and VEGFR1$^+$VLA-4$^+$ clusters dictate organ-specific tumour spread.

Bone marrow-derived cells (BMDCs) contribute to malignant transformation1, tumour vascularization2,3 and neoplastic cell migration4. Previously, we identified haematopoietic progenitor cells (HPCs) expressing VEGFR1 that reside within specified niches of the bone marrow. During the angiogenic switch, these cells proliferate and mobilize to the bloodstream along with bone marrow-derived endothelial progenitor cells that express VEGFR2 (also known as Flk1), and contribute to the vascularization and growth of specific primary tumours[2,5]. These myelomonocytic VEGFR1$^+$ cells localize to perivascular sites, thus stabilizing tumour neo-vessels[2]. These and other tumour-associated cells enhance primary tumour neo-angiogenesis and growth, yet their precise contribution to metastasis is unclear[6–8]. Therefore, the aim of this study was to determine the role of VEGFR1$^+$ HPCs in the temporal and functional generation of metastasis.

BMDCs colonize pre-metastatic sites before tumour cells

We analysed the fate of β-galactosidase-positive (β-gal$^+$) and green fluorescent protein-positive (GFP$^+$) BMDCs following intradermal primary tumour injection in mice. Animals were inoculated with either Lewis lung carcinoma (LLC) cells, which metastasize to the lungs and occasionally the liver, or B16 melanoma cells, which possess a more widely disseminated metastatic potential. After irradiation, but before tumour implantation, we observed minimal β-gal$^+$ BMDCs (mean ± s.e.m., 0.01% ± 0.01 of cells β-gal$^+$ per ×100 objective field) or GFP$^+$ BMDCs in the lungs. (Fig. 1a, b, left panels). By day 14 after tumour implantation, but before the arrival of tumour cells, the extravasation and cluster formation of β-gal$^+$ BMDCs (3.2% ± 1.2, $P < 0.05$ by Student's *t*-test) or GFP$^+$ BMDCs were detected near terminal bronchioles and distal alveoli, both common sites for future tumour metastasis (Fig. 1a, b, left middle panels and insets). On day 16, established β-gal$^+$ cell clusters dictated the contours of future metastatic lesions (Fig. 1a, right middle panel). Individual DsRed-tagged tumour cells, associated with pre-existing BMDC clusters, were visible by day 18 (Fig. 1b, right middle panel) and progressed to micrometastases by day 23 (Fig. 1a, b, right panels). β-gal$^+$ BMDCs were maintained within well-established tumour metastases (Fig. 1a, right panel and inset).

To further define the timing of tumour cell arrival, a flow cytometric study of the lungs was undertaken. Before day 8, minimal GFP$^+$ BMDCs were observed in this tissue; however, from day 12, BMDCs began migrating into the lung (Fig. 1c, graph and left flow cytometry panel). These GFP$^+$ cells increased in number, and were joined by DsRed-tagged tumour cells by day 18 (Fig. 1c, graph and right flow diagram). No tumour cells were detected by flow cytometry or microscopy earlier than day 16, and increasing numbers of tumour cells were identified over time (Fig. 1b, right panels; Fig. 1c; Supplementary Fig. 1a). More than 95% of tumour cells co-clustered with GFP$^+$ BMDCs (97% ± 1.1; Fig. 1b, right panels).

Although a few tumour cells may have been undetectable using these methodologies, further experiments in mice given B16-melanoma-conditioned media (MCM) showed that this conditioning alone mobilized BMDCs that were capable of forming a pre-metastatic niche. We introduced DsRed-tagged B16 tumour cells intravenously into mice with pre-established GFP$^+$ BMDC clusters in the lung after challenge with MCM (Fig. 1d, right panel) or media alone (Fig. 1d, left panel). MCM increased the number of tumour cells in the lung one day after

tumour injection compared with media alone (141.3 ± 10.2 versus 2.7 ± 0.6 tumour cells per section of lung tissue, $P < 0.01$). Four days after tumour injection, the frequency and size of the lung nodules were augmented by MCM (207 ± 5.6 versus 14 ± 1.7, $P < 0.01$; Fig. 1d, right panel inset). Co-localization of DsRed-tagged tumour cells with GFP^+ BMDC clusters was >93% at both time points, indicating that BMDCs assist tumour cell adhesion and proliferation. Therefore, factors provided by the primary tumour induce BMDCs to enter the bloodstream and mobilize to organ-specific pre-metastatic sites, and this migration precedes the arrival of tumour cells.

Sites of BMDC clusters are tumour-type specific

We examined whether the type of tumour cell dictated BMDC distribution to specific pre-metastatic sites. Intradermal injection of LLC cells resulted in BMDC cluster formation limited to the lung (47.5 ± 2.6 clusters per ×100 objective field) and liver (10.8 ± 1.1) with no clusters in other organs (Fig. 1e, left panel). In contrast, the B16 melanoma tumour cells induced the formation of BMDC clusters in multiple tissues such as the lung (103.8 ± 6.9), liver (41.8 ± 2.4), testis (36.6 ± 3.1), spleen (25 ± 3.2) and kidney (20.6 ± 1.8), which are all common metastatic sites for this tumour (Fig. 1e, right panel). Furthermore, melanoma cells, consistent with their more aggressive metastatic nature, induced more clusters than LLC cells ($P < 0.01$).

Recruited BMDCs consist of haematopoietic progenitors

We characterized the cellular and molecular composition of incorporated BMDC clusters. Clusters induced by either tumour type expressed VEGFR1 (Fig. 2a, right panel), and GFP^+ BMDC clusters coexpressed VEGFR1 (Fig. 2b, left panel), compared with little VEGFR1 in the lung after irradiation alone (Fig. 2a, left panel and inset). Further characterization revealed that subsets of $VEGFR1^+$ BMDCs coexpressed the stem/progenitor cell antigens CD133 (Fig. 2b, right panel), CD34 (Supplementary Fig. 1b and Supplementary Table) and CD117 (also known as c-Kit; Fig. 2c), suggesting that these cells may comprise phenotypically marked $VEGFR1^+$ HPCs and precursor cells. After primary tumour implantation, CD117-positive progenitor cells arrived in the lung before GFP-tagged tumour cells by flow cytometry (Supplementary Fig. 1c), recapitulating the recruitment of BMDCs described above. There is a degree of maturational heterogeneity, with the myelomonocytic marker CD11b present on certain incorporated cells (data not shown). Early $VEGFR1^+$ bone marrow clusters lacked expression of VEGFR2 and CD31 (also known as PECAM1; Supplementary Fig. 1d, left and left middle panels, respectively). VEGFR2-positive circulating endothelial progenitor cells migrated to fully formed BMDC clusters (Supplementary Fig. 1d, right panel), and coincided with the arrival of tumour cells (Supplementary Fig. 1e, graph). Thus bone marrow-derived $VEGFR1^+$ HPCs initiate and maintain the pre-metastatic niche.

BMDC clusters occur in a spontaneous tumour model

We compared these findings to those in a spontaneous tumour model using c-Myc transgenic mice. On day 40 of life, prominent $VEGFR1^+$ clusters were detected exclusively in the lymph nodes of these animals before the onset of lymphoma (145.1 ± 16.4 clusters per ×100 objective field; Fig. 2d, middle panel and inset), with no observed clusters in wild-type littermates (0.4 ± 0.3, $P < 0.001$; Fig. 2d, left panel). By 120 days, $VEGFR1^+$ clusters persisted in established lymphomas (67.8 ± 9.5 versus 0.7 ± 0.5 in c-Myc mice versus littermates, $P < 0.001$; Fig. 2d, right panel and inset). The lymphoma cells, which surrounded the $VEGFR1^+$ HPCs, did not express VEGFR1 (Fig. 2d, right panel inset).

BMDC clusters are recruited to pre-metastasic human tissue

To validate the mouse data showing tumour-specific formation of VEGFR1$^+$ cellular clusters, we analysed human tissues from patients with malignancy. VEGFR1$^+$ clusters were observed in both primary tumours and metastatic tissue (Fig. 3, showing breast carcinoma in an axillary lymph node, lung carcinoma and oesophageal carcinoma). There were increased cellular clusters in common sites of metastasis before tumour spread, suggesting the potential of this tissue as a future site for metastasis (Fig. 3, showing axillary lymph node (21 ± 5 clusters per ×100 objective field), lung (19 ± 4) and gastro-oesophageal junction (25 ± 4)). In patients without malignancy, lymph nodes and lung tissue did not show VEGFR1$^+$ clusters (Fig. 3b, d, insets). VEGFR1$^+$ cellular clusters expressed the haematopoietic progenitor marker c-Kit (Fig. 3e, f, insets).

Functional role for VEGFR1$^+$ BMDCs in directing metastasis

We assessed the potential of purified VEGFR1$^+$ bone marrow cells to initiate pre-metastatic clusters by selectively transplanting these progenitors into irradiated mice. By day 24 after LLC tumour cell implantation, control mice that received wild-type bone marrow showed prominent lung metastases and established blood vessels (Fig. 4a, left panel and inset). However, mice transplanted with purified VEGFR1$^+$ cells formed numerous micrometastases throughout the lungs (25 ± 9 micrometastases per ×100 objective field; Fig. 4a, middle panel) with aberrant vasculature (Fig. 4a, middle panel inset). In contrast, bone marrow depleted of VEGFR1$^+$ cells failed to produce pre-metastatic clusters (Fig. 4a, right panel; $P < 0.01$ by analysis of variance (ANOVA)). These results suggest that the VEGFR1$^+$ HPCs initiating the pre-metastatic cluster can attract tumour cells.

To address whether disruption of VEGFR1$^+$ cellular cluster formation could block the metastasis of well-established tumours, mice inoculated with LLC or B16 tumour cells were treated with monoclonal antibodies against VEGFR1 and/or VEGFR2. This approach allows for selective targeting of the BMDCs, as the tumour cells do not express either VEGFR1 or VEGFR2. By day 24, widespread metastases were evident in untreated mice with LLC tumours in the lung (Fig. 4b, left panel) or B16 tumours in the spleen (Supplementary Fig. 2, left panel and inset). Anti-VEGFR1 antibody treatment eliminated the initiating clusters and completely prevented metastasis (Fig. 4b, left middle panel; Supplementary Fig. 3; $P < 0.01$ by ANOVA), whereas anti-VEGFR2 antibody did not prevent the formation of VEGFR1$^+$ clusters but limited metastatic progression (15 ± 11 micrometastases per ×100 objective field; Fig. 4b, right middle panel and inset; Supplementary Fig. 3). The two antibodies combined blocked cluster formation to an extent similar to anti-VEGFR1 therapy; however, we did observe an isolated LLC lesion in the lung of one animal (Supplementary Fig. 3b, inset). Collectively, these results suggest that targeting the VEGFR1$^+$ cell cluster can prevent tumour cell adhesion, proliferation and metastatic spread.

VLA-4, MMP9 and Id3 mediate the pre-metastatic niche

We investigated the cellular and molecular mechanisms by which migratory HPCs, through interaction with the microenvironment, form permissive pre-metastatic niches. The interaction of VLA-4 (integrin $\alpha_4\beta_1$) with its ligand fibronectin is essential for the migration of haematopoietic cells within the bone marrow[9,10] and of circulating leukocytes[4,11]. We assessed whether VEGFR1$^+$ cells express integrins, which may facilitate the interaction of this cell type with the pre-metastatic niche. We found that VEGFR1$^+$ HPCs at the pre-metastatic cluster express VLA-4 (Fig. 5a, and inset showing coexpression with VEGFR1), suggesting that VLA-4 allows for the adhesion of the BMDCs that form the pre-metastatic niche. Following cluster formation, $\alpha_4\beta_7$ and $\alpha_6\beta_4$ integrins were prominently expressed within the metastatic niche (data not shown). Proteinases including matrix metalloproteinase 9 (MMP9), produced

by haematopoietic cells, can serve to break down basement membranes, thus altering the local microenvironments by releasing soluble Kit-ligand and VEGF-A to support newly introduced cells that express c-Kit[12,13]. In addition, metalloproteinase expression can be enhanced through $\alpha_4\beta_1$ signalling after fibronectin binding[14,15]. MMP9 was expressed in pre-metastatic clusters, and this upregulation of MMP9 expression may be a result of integrin binding and activation in VEGFR1$^+$ HPCs (Fig. 5b). These findings expand upon previous work demonstrating that VEGFR1-mediated induction of MMP9 directed metastasis to the lungs[7].

We previously showed that upregulation of Id gene expression is critical for the mobilization of progenitors that aid the growth of primary tumours[15]. Id3 expression was also seen within the clusters (Fig. 5c, and inset showing coexpression with VEGFR1). Id3 may facilitate the mobilization of VEGFR1$^+$ cells to the pre-metastatic niche. In addition, expression of specific integrins is regulated by Id genes, and may be responsible for BMDC and stromal cell interactions, motility and recruitment[16].

To confirm the functional roles of these proteins in establishing the pre-metastatic niche, we either inhibited the expression of VLA-4 (with anti-integrin α4 antibodies) or studied VEGFR1$^+$ cell cluster formation in MMP9 and Id3 knockout mice. In these models, we found reduced cluster formation (Supplementary Fig. 3a–c) and metastatic spread three weeks after tumour implantation. We also found impaired mobilization of VEGFR1$^+$ HPCs into the circulation of Id3 knockout mice compared to wild type (654 versus 3,283 VEGFR1$^+$ CD11b$^+$ cells μl^{-1}) in response to tumour inoculation ($P < 0.01$ by Student's t-test; Supplementary Table). Decreased mobilization of HPCs may explain the reduced metastatic phenotype seen in these animals[2,17].

To formally examine the potential of wild-type VEGFR1$^+$ cells to restore the metastatic defect in Id3 knockout mice, Id3-competent GFP$^+$VEGFR1$^+$ HPCs were injected intravenously into Id3 knockout tumour-bearing mice. VEGFR1$^+$ HPCs alone re-established cluster formation and micrometastases by day 21 after tumour implantation (Fig. 5d, and upper inset; Supplementary Fig. 3c). Notably, the LLC metastatic lesions were associated with GFP$^+$BMDCs (Fig. 5d, lower inset). These findings further emphasize the functional role of VEGFR1$^+$ BMDCs in the establishment of clusters and metastasis.

Fibronectin upregulation supports adhesion of VLA-4$^+$ BMDCs

We next investigated the potential of tissue-specific ligands to support the adhesion and formation of BMDC clusters. Following the implantation of LLC tumour cells, but before the homing of the VLA-4$^+$VEGFR1$^+$ BMDCs, increased fibronectin expression was observed from day 3 (Fig. 5e, middle panel; Fig. 5f) to day 14 (Fig. 5e, right panel; Fig. 5f) in the vicinity of the future metastatic niche, compared with the baseline level of fibronectin expression in wild-type lung (Fig. 5e, left panel; Fig. 5f). Furthermore, resident fibroblast-like stromal cells (Fig. 5e, left panel inset), which proliferate in response to primary tumour (Fig. 5e, right panel inset), may contribute to the localized deposition of fibronectin. Melanoma cells also induced fibronectin expression in the lung in a similar fashion to that of LLC cells (Supplementary Fig. 3d). Moreover, increased fibronectin expression was notable in multiple tissues exposed to MCM, such as the intestine and oviduct, consistent with the more aggressive metastatic nature of B16 cells (fibronectin expression: $P < 0.05$ days 3–5 and $P < 0.001$ days 7–9 (by ANOVA) in oviducts (Fig. 6a) and intestines (Fig. 6b) with MCM treatment compared with mice treated with LLC-conditioned media (LCM) or wild-type mice).

VEGFR1$^+$ cells promote tumour adherence and growth

To confirm that VEGFR1$^+$ progenitors promote the chemoattraction and attachment of circulating tumour cells, we isolated and red fluorescence-labelled (PKH26-Gl) VEGFR1$^+$

cells from mice with malignancy (Supplementary Fig. 4). Within one hour of *in vitro* co-incubation with green fluorescence-labelled (PKH2-GL) B16 or LLC cells, the HPCs aggregated, proliferated (150% increase) and promoted the attachment and proliferation of the tumour cells. In contrast, preculturing VEGFR1$^+$ HPCs with either anti-VEGFR1 or anti-VLA-4 antibodies blocked this binding affinity and expansion (Supplementary Fig. 4a, middle and right panels). Using a transwell migration assay, tumour cells manifested enhanced mobility in response to bone marrow-derived VEGFR1$^+$ cells (29.6 ± 1.4 tumour cells per ×200 objective field) as compared to cells that do not express VEGFR1 (11.2 ± 0.4) and media alone (9.9 ± 0.9, $P < 0.001$ by ANOVA; Supplementary Fig. 4b). The SDF-1/CXCR4 chemokine axis participates in homing and retention of HPCs within the bone marrow[18]. Specific tumour cell types, which express CXCR4, may also migrate in this fashion in response to local chemokine gradients[19–21]. Within the fully formed pre-metastatic cluster containing VEGFR1$^+$ cells, fibroblasts and fibronectin (Fig. 1a, left middle panel), SDF-1 (also known as CXCL12) became highly expressed (Supplementary Fig. 4c). We also observed CXCR4 expression in B16 melanoma and LLC tumours (Supplementary Fig. 4d). These data suggest that SDF-1 may provide one pathway for attracting CXCR4$^+$ tumour cells to the pre-metastatic niche.

Tumour-derived conditioned media dictate metastatic patterns

To delineate the mechanism of the organ-specific metastatic potential of LLC and B16 cells, we collected culture-derived conditioned media. Similarly, but more rapidly than primary LLC cells, the intraperitoneal injection of LCM generated fibronectin expression, possibly from resident fibroblasts, and BMDC cluster formation (Supplementary Fig. 5a) compared with media alone (Supplementary Fig. 5a, insets). MCM stimulated fibronectin expression to a greater extent in liver than LCM (Supplementary Fig. 5b). MCM caused enhanced fibroblast proliferation (data not shown) and fibronectin expression with cluster formation in a wide range of organs, as shown for intestine (Fig. 6a, b; Supplementary Fig. 5b) in comparison to media (Supplementary Fig. 5b, inset). We analysed LCM and MCM for variations in growth factors to account for the distinct metastatic potentials and profiles of LLC and B16 (Fig. 6c). We found high levels of VEGF in both conditioned media, more than in plasma from tumour-bearing mice (Supplementary Fig. 5c). However, in MCM and melanoma-derived plasma we specifically detected higher levels of placental growth factor (PlGF), which signals though VEGFR1 alone, as compared with LCM- and LLC-derived plasma (Fig. 6c, Supplementary Fig. 5c). Furthermore, in the low-metastatic-variant of LLC, levels of both VEGF and PlGF were much lower in the conditioned media (L-LCM) and plasma compared with its more aggressive counterpart (Fig. 6c, Supplementary Fig. 5c). In a transwell assay, LCM and MCM enhanced the migration of VEGFR1$^+$ BMDCs most effectively when compared with the other growth factor conditions (LCM 55% ± 0.4, MCM 68.1% ± 5, media 10.8% ± 1.7, $P < 0.001$ by ANOVA; Fig. 6d). Considering these results, we questioned whether cytokines such as PlGF present in MCM were capable of redirecting LLC metastases to non-conventional metastatic sites for this tumour. MCM given before intradermal LLC implantation, and daily thereafter, resulted in the redirection of LLC metastasis from lung to those sites frequently observed in melanoma including kidney, spleen, intestine and oviduct (Fig. 6e). Our results demonstrate that tumour-specific chemokines and/or cytokines present in conditioned media, along with the VEGFR1$^+$ cellular clusters, are another determinant in the multidimensional programme driving metastatic spread.

The precise cellular and molecular mechanisms that dictate metastasis of a specific tumour to a predetermined metastatic location are not known. Many tumours have a predilection for metastasis to specific organs. Based on the current dogma, metastatic predisposition is believed to reflect inherent molecular differences in tumour cells themselves and the potential influence by surrounding stromal cells, which include the vasculature, connective tissue and immune

cells[22–26]. Our results introduce the concept that tumour metastasis is initiated by a well-defined sequence of events dependent on cellular 'bookmarking' through site-specific delivery of VEGFR1$^+$ cells to form permissive niches within target organs. Our data suggest that differences in tumour-secreted humoral factors promote metastatic spread in specific distant organs. Within days following tumour implantation, fibronectin becomes upregulated in certain locations by resident fibroblast and fibroblast-like cells within target organs that are conventional sites of metastasis, corresponding to the particular primary tumour. Simultaneously, HPCs exit the bone marrow into the peripheral circulation as previously described[11]. As a result of the niche-specific directional cues from fibronectin, VEGFR1$^+$ HPCs, expressing VLA-4 and Id3, can traverse established endothelium to form a pre-metastatic niche before the arrival of CXCR4$^+$ tumour cells and VEGFR2$^+$ endothelial cells. These clusters, with MMP9 production altering the microenvironment and enhanced expression of SDF-1 creating a chemokine gradient, permit the attraction of tumour cells and their incorporation into the niche, thereby developing a complete metastatic lesion. We show that inhibition by a VEGFR1 antibody or depletion of VEGFR1$^+$ cells from the bone marrow prevents the formation of pre-metastatic clusters and, therefore, metastases. Moreover, blocking either VEGFR1 or VLA-4 inhibits the binding and establishment of the haematopoietic cell clusters and tumour cells. Restoration of the pre-metastatic niche and metastasis with the introduction of wild-type VEGFR1$^+$ cells into Id3 knockout mice suggests that the expression of Id3 induces expression of the necessary elements, including MMP9, integrins and possibly chemokines, to provide a road map for the homing of VEGFR1$^+$ cells essential for the establishment of the pre-metastatic niche.

Much focus has been placed on the role of inflammatory cells in aiding in tumour adherence and invasion into distant organs[27–30]. The VEGFR1$^+$ HPCs identified in this study show characteristics common to physiological pathways of inflammation by providing the necessary adhesion molecules, proteinases, chemokines and growth conditions to create a conducive microenvironment for engraftment of tumour cells[12,20,31]. The pre-metastatic niche, however, is distinct, introducing an undifferentiated state as seen with the VEGFR1$^+$ HPC population. This is the first direct evidence that a non-neoplastic cell population can portend a future metastatic site. Furthermore, identification of haematopoietic clusters in human tissues before evidence of tumour spread demonstrates the applicability of targeting VEGFR1 and VLA-4 to identify and prevent metastasis in the clinical setting. This concept will have a tremendous impact on tumour staging, and may alter the landscape of adjuvant chemotherapy.

METHODS

Bone marrow transplantation

Wild-type C57Bl/6 mice were lethally irradiated (950 rads) and transplanted with 1×10^6 β-gal$^+$ bone marrow cells (from Rosa26 mice) or 1×10^6 GFP$^+$ bone marrow cells (from EGFP-transgenic mice, C57Bl/6-TgN(ActbEGFP)1Osb/J; Jackson Laboratory)[2]. After 4 weeks, mice were injected intradermally in the flank with either 2×10^6 LLC or B16 cells (American Type Culture Collection).

Selective bone marrow transplantation

Mice irradiated as described above received a bone marrow transplant from purified cell populations obtained as described in the Supplementary Methods.

β-Galactosidase staining

Tissues and femoral bones were fixed in 4% paraformaldehyde for 4 h. The samples were stained in 5-bromo-4-chloro-3-indolyl-β-D-galactoside (X-gal) solution at 37 °C, as described[32], for 36 h and then embedded2.

GFP visualization

Tissues were immediately frozen in OCT compound (Tissue-Tek) without fixation. Serial sections (cryostat, Leica) were mounted with Vectashield containing DAPI (4,6-diamidino-2-phenylindole), and visualized with an ultraviolet fluorescent microscope (Nikon Eclipse E800) with a Retiga camera (QImaging) through IPLab version 3.65a imaging software (Scanalytics).

Immunohistochemistry

Tissues were fixed and embedded in OCT or paraffin as previously described[16]. The following antibodies were used: VEGFR1 clone MF-1 (ImClone Systems) or Flt1 clone C-17 (Santa Cruz Biotechnology); CD31 SC-1506 (Santa Cruz Biotechnology); VEGFR2 DC101 (ImClone Systems); MMP9 D19557 (Oncogene); Id3 C-20 (Santa Cruz Biotechnology); Fibronectin TV-1 (Chemicon); CD11b CBRM1/5 (eBioscience); CD34 RAM34 (BD Pharmigen); c-Kit ACK2 (eBioscience); PDGFRα APA5 (BD Pharmingen); αV (Chemicon); CD133 13A4 (eBioscience); α4/VLA-4 PS-2 (Southern Biotech); α5 (CD49e, 5H10-27); α6/CD49f GoH3 (BD Pharmingen); β1 9EG7 (BD Pharmingen); β2 M18/2 (BD Pharmingen); β4 (Santa Cruz Biotechnology); β7 M293 (BD Pharmingen); SDF-1 79018.111 (R&D Systems); and CXCR4 2B11 (BD Pharmingen).

Double immunofluorescence

Tissues in OCT were post-fixed with acetone. A double immunofluorescence protocol was performed as described in the Supplementary Methods.

Antibody targeting

Wild-type mice were inoculated with 2×10^6 LLC or B16 cells. For blockade of VEGFR1 function, mice were injected intraperitoneally every 48 h, between day 7–22, with rat anti-mouse VEGFR1 antibody (MF-1, IgG1, 400 μg, ImClone Systems) or VEGFR2 antibody (DC101, IgG1, 800 μg, ImClone Systems) or both, or with IgG control antibody, and then killed on day 24.

Conditioned media assays

Conditioned media was filtered (0.22-μm filter) from serum-free media cultured on B16 (MCM) or LLC (LCM) cells for 18 h, as described[33]. Conditioned media (300 μl) was injected intraperitoneally daily for nine days into wild-type mice that had received Rosa26 bone marrow transplants four weeks earlier. Tissues were stained for fibronectin TV-1 (Chemicon) and β-gal. For tumour redirection studies, intraperitoneal injections of MCM (300 μl) commenced two days before intradermal LLC implantation and then daily over the next 21 days. Matched control groups with and without tumour were given serum-free media. Wild-type mice were injected with MCM (300 μl) daily for seven days before tail vein injection of B16 tumour cells, and then daily until killed either one or four days after intravenous tumour administration. Lungs were perfused with PBS before embedding in OCT.

Migration assays

Migration of $VEGFR1^+$ cells in response to conditioned media was measured in a transwell assay. $VEGFR1^+$ cells were isolated as above, and 1×10^5 cells suspended in serum-free media placed in the upper compartment of 5-μm-pore transwells (Costar, Corning). Cells were allowed to migrate for 18 h with conditioned media or corresponding control media in the lower compartment, with the analysis of cell counts assessed every 6 h using a haemocytometer and trypan blue.

Quantitative analysis of fibronectin expression

Lung tissue was homogenized with a tissue homogenizer in TriZol reagent, and RNA was extracted as described previously[34]. Fibronectin gene expression was quantified and normalized to glyceraldehyde-3-phosphate dehydrogenase (*Gapdh*) expression by polymerase chain reaction with reverse transcription (RT–PCR) using TaqMan gene expression assays (Applied Biosystems) as described previously[35]

Chemokine assays

Conditioned media, serum-free media and plasma obtained from mice with day 14 tumours were analysed for VEGF and PlGF concentrations by an enzyme-linked immunosorbent assay (ELISA; Quantikine, R&D Systems) according to the manufacturer's instructions.

Flow cytometry

Flow cytometry was performed on an entire right lung after perfusion with PBS by right-ventricular injection. The tissue was minced into small pieces, filtered with 100- and 40-μm filters (BD Biosciences) to form a single-cell suspension as previously described[35,36].

Human specimens

Human specimens include: tumour tissue, adjacent normal tissue (beyond tumour margins), distant normal tissue and lymph nodes. Tissues were embedded as described above and stained with antibodies to human VEGFR1 FB5 (ImClone Systems) or Flt1 (Calbiochem). Tissue samples were obtained and handled in accordance with an approved Institutional Review Board application.

Quantitative immunohistochemistry

Using both IPLab and Adobe Photoshop 7.0, random ×100 objective fields were analysed by selecting a standardized colour range for β-gal or immunohistochemical staining. After boundary delineation, the area under the pixelation histogram was calculated, comparing total staining area to total tissue area.

Statistical analyses

Results are expressed as mean ± s.e.m. Data were analysed by Student's *t*-test and one way analysis of variance (ANOVA) using the GraphPad Prism statistical program. *P* values <0.05 were considered significant. Error bars depict s.e.m.

Supplementary Material

Refer to Web version on PubMed Central for supplementary material.

Acknowledgments

We thank M. Barna for critical reading of the manuscript and L. Breda, S. Rivella and S. Neustein for discussions. R.N.K. is a recipient of the Laura Rosenberg Fellowship award and supported by a grant from the American Hellenic Educational Progressive Association (Fifth District) and the LTC Foundation. D.L. is supported by the Doris Duke Charitable Foundation, the Children's Blood Foundation, the Emerald Foundation, the Theodore A. Rapp Foundation and a grant from the National Cancer Institute. S.R. is an investigator of the Howard Hughes Medical Institute and supported by grants from the American Cancer Society, the Leukemia and Lymphoma Society, and the National Institutes of Health.

References

1. Coussens L, Tinkle C, Hanahan D, Werb Z. MMP-9 supplied by bone marrow-derived cells contributes to skin carcinogenesis. Cell 2000;103:481–490. [PubMed: 11081634]
2. Lyden D, et al. Impaired recruitment of bone-marrow-derived endothelial and hematopoietic precursor cells blocks tumour angiogenesis and growth. Nature Med 2001;7:1194–1201. [PubMed: 11689883]
3. Autiero M, Luttun A, Tjwa M, Carmeliet P. Placental growth factor and its receptor, vascular endothelial growth factor receptor-1: novel targets for stimulation of ischemic tissue revascularization and inhibition of angiogenic and inflammatory disorders. J. Thromb. Haemost 2003;1:1356–1370. [PubMed: 12871269]
4. Neeson P, Thurlow P, Jamieson G, Bradley C. Lymphocyte-facilitated tumour cell adhesion to endothelial cells: the role of high affinity leukocyte integrins. Pathology 2003;35:50–55. [PubMed: 12701685]
5. Hattori K, et al. Placental growth factor reconstitutes hematopoiesis by recruiting VEGFR1^{+} stem cells from bone-marrow microenvironment. Nature Med 2002;8:841–849. [PubMed: 12091880]
6. Pollard JW. Tumour-educated macrophages promote tumour progression and metastasis. Nature Rev. Cancer 2004;4:71–78. [PubMed: 14708027]
7. Hiratsuka S, et al. MMP9 induction by vascular endothelial growth factor receptor-1 is involved in lung-specific metastasis. Cancer Cell 2002;2:289–300. [PubMed: 12398893]
8. De Palma M, Vinneri MA, Roca C, Naldini L. Targeting exogenous genes to tumour angiogenesis by transplantation of genetically modified hematopoietic cells. Nature Med 2003;9:789–795. [PubMed: 12740570]
9. Burger J, Spoo A, Dwenger A, Burger M, Behringer D. CXCR4 chemokine receptors (CD184) and $\alpha_4\beta_1$ integrins mediate spontaneous migration of human CD34^{+} progenitors and acute myeloid leukaemia cells beneath marrow stromal cells (pseudoemperipolesis). Br. J. Haematol 2003;122:579–589. [PubMed: 12899713]
10. Scott L, Priestly G, Papayannopoulou T. Deletion of α_4 integrins from adult hematopoietic cells reveals roles in homeostasis, regeneration, and homing. Mol. Cell. Biol 2003;23:9349–9360. [PubMed: 14645544]
11. Jonjic N, et al. Molecules involved in the adhesion and cytotoxicity of activated monocytes on endothelial cells. J. Immunol 1992;148:2080–2083. [PubMed: 1347549]
12. Heissig B, et al. Recruitment of stem and progenitor cells from the bone marrow niche requires MMP-9 mediated release of kit-ligand. Cell 2002;109:625–637. [PubMed: 12062105]
13. Bergers G, et al. Matrix Metalloproteinase-9 triggers the angiogenic switch during carcinogenesis. Nature Cell Biol 2000;2:737–744. [PubMed: 11025665]
14. Huhtala P, et al. Cooperative signalling by α5β1 and α4β1 integrins regulates metalloproteinase gene expression in fibroblasts adhering to fibronectin. J. Cell Biol 1995;129:867–879. [PubMed: 7537277]
15. Yakubenko VP, Lobb RR, Plow EF, Ugarova TP. Differential induction of gelatinase B (MMP-9) and gelatinase A (MMP-2) in T lymphocytes upon $\alpha_4\beta_1$-mediated adhesion to VCAM-1 and the CS-1 peptide of fibronectin. Exp. Cell Res 2000;260:73–84. [PubMed: 11010812]
16. Ruzinova MB, et al. Effect of angiogenesis inhibition by Id loss and the contribution of bone-marrow-derived endothelial cells in spontaneous murine tumours. Cancer Cell 2003;4:277–289. [PubMed: 14585355]
17. Lyden D, et al. Id1 and Id3 are required for neurogenesis, angiogenesis and vascularization of tumour xenografts. Nature 1999;401:670–677. [PubMed: 10537105]
18. Ratajczak MZ, et al. Stem cell plasticity revisted: CXCR4-positive cells expressing mRNA for early muscle, liver and neural cells 'hide out' in the bone marrow. Leukemia 2004;18:29–40. [PubMed: 14586476]
19. Lapidot T, Petit I. Current understanding of stem cell mobilization: The roles of chemokines, proteolytic enzymes, adhesion molecules, cytokines and stromal cells. Exp. Hematol 2002;30:973–981. [PubMed: 12225788]
20. Balkwill F. The significance of cancer cell expression of the chemokine receptor CXCR4. Semin. Cancer Biol 2004;14:171–179. [PubMed: 15246052]

21. Muller A, et al. Involvement of chemokine receptors in breast cancer metastasis. Nature 2001;410:50–56. [PubMed: 11242036]
22. Hynes RO. Metastatic potential: generic predisposition of the primary tumour or rare, metastatic variants—or both? Cell 2003;113:821–823. [PubMed: 12837240]
23. Bergers G, Song S, Meyer-Morse N, Bergsland E, Hanahan D. Benefits of targeting both pericytes and endothelial cells in the tumour vasculature with kinase inhibitors. J. Clin. Invest 2003;111:1287–1295. [PubMed: 12727920]
24. Fidler I. The organ microenvironment and cancer metastasis. Differentiation 2002;70:498–505. [PubMed: 12492492]
25. Duda DG, et al. Differential transplantability of tumour-associated stromal cells. Cancer Res 2004;64:5920–5924. [PubMed: 15342367]
26. Folkman J. Role of angiogenesis in tumour growth and metastasis. Semin. Oncol 2002;29:515–518.
27. Coussens LM, Werb Z. Inflammation and cancer. Nature 2002;420:860–867. [PubMed: 12490959]
28. Borsig L, Wong R, Hynes RO, Varki NM, Varki A. Synergistic effects of L- and P-selectin in facilitating tumour metastasis can involve non-mucin ligands and implicate leukocytes as enhancers of metastasis. Proc. Natl Acad. Sci. USA 2000;99:2193–2198. [PubMed: 11854515]
29. Lin EY, Ngyuen AV, Russell RG, Pollard JW. Colony stimulating factor 1 promoted progression of mammary tumours to malignancy. J. Exp. Med 2001;193:727–740. [PubMed: 11257139]
30. Qian F, Hanahan D, Weissman IL. L-selectin can facilitate metastasis to lymph nodes in a transgenic mouse model of carcinogenesis. Proc. Natl Acad. Sci. USA 2002;98:3976–3981. [PubMed: 11274419]
31. Schoppmann S, et al. Tumour-associated macrophages express lymphatic endothelial growth factors and are related to peritumoural lymphangiogenesis. Am. J. Pathol 2002;161:947–956. [PubMed: 12213723]
32. Tam PP, Parameswaran M, Kinder SJ, Weinberger RP. The allocation of epiblast cells to the embryonic heart and other mesodermal lineages: the role of ingression and tissue movement during gastrulation. Development 1999;124:1631–1642. [PubMed: 9165112]
33. Kessinger A, Mann S, Murphy BO, Jackson JD, Sharp JG. Circulating factors may be responsible for murine strain-specific responses to mobilizing cytokines. Exp. Hematol 2001;29:775–778. [PubMed: 11378273]
34. Hashimoto N, Jin H, Liu T, Chensue SW, Phan SH. Bone marrow-derived progenitor cells in pulmonary fibrosis. J. Clin. Invest 2004;113:243–252. [PubMed: 14722616]
35. Jensen KK, et al. The human herpes virus 8-encoded chemokine receptor is required for angioproliferation in a murine model of Kaposi's sarcoma. J. Immunol 2005;174:3686–3694. [PubMed: 15749907]
36. Huaux F, Tianju L, McGarry B, Ullenbruch M, Phan SH. Dual roles of IL-4 in lung injury and fibrosis. J. Immunol 170:2083–2092. [PubMed: 12574379]

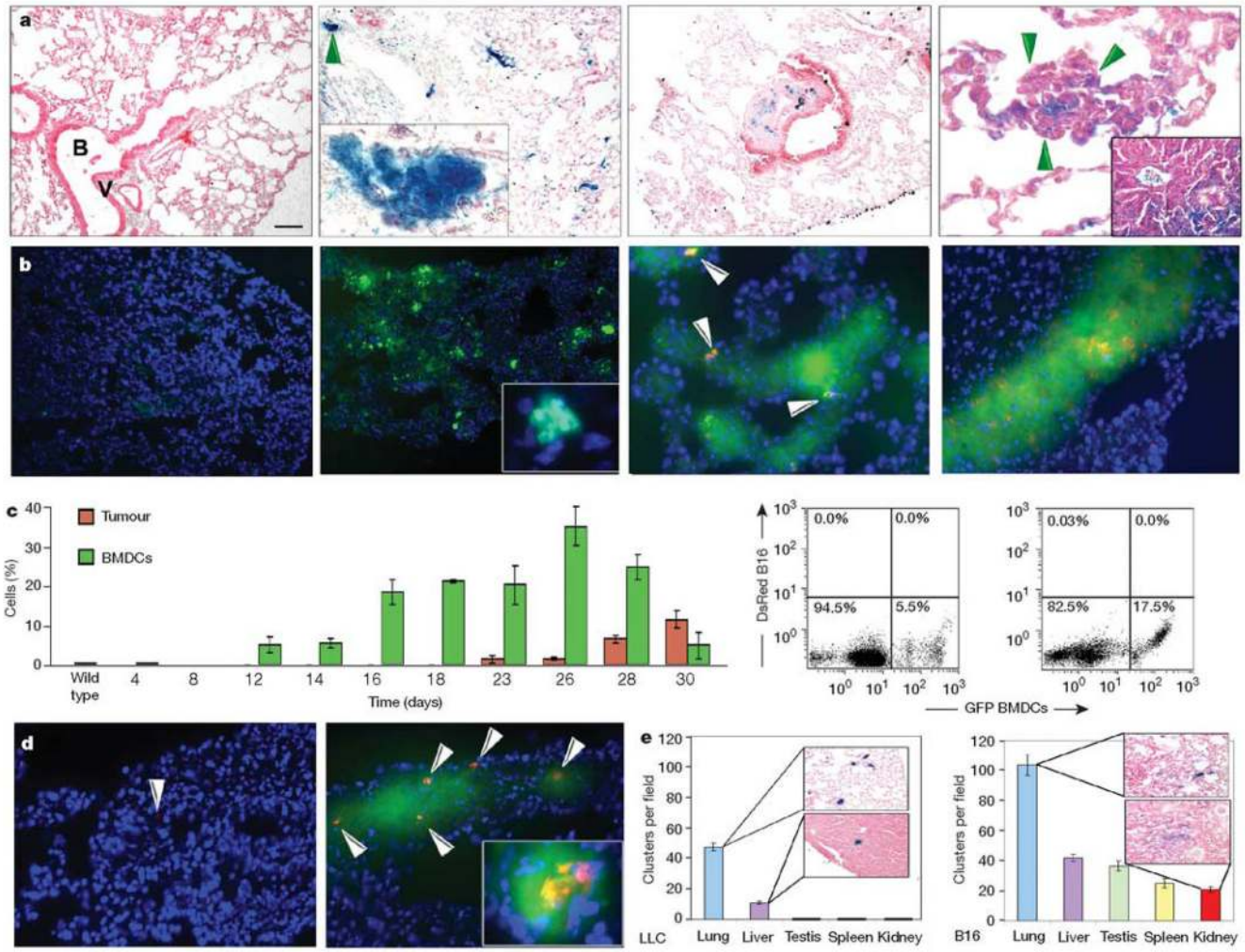

Figure 1. Bone marrow-derived cells form the pre-metastatic niche

a, β-gal$^+$ bone marrow cells (left panel) are rarely observed in lungs after irradiation and before LLC cell implantation ($n = 6$). By day 14, β-gal$^+$ bone marrow-derived clusters appear in the lung parenchyma (left middle panel and magnified inset of the region arrowed; $n = 25$) and are associated with micrometastases by day 23 (right panel, arrows) and in gross metastases (right panel, inset; $n = 12$). Also shown is a cluster with associated stroma between a terminal bronchiole and bronchial vein, a common metastatic site (right middle panel). B, terminal bronchiole; V, bronchial vein. **b**, GFP$^+$ bone marrow in the lungs after irradiation and before DsRed-tagged B16 cell implantation (left panel; $n = 6$). On day 14, GFP$^+$ (green) BMDCs are seen with no DsRed$^+$ (red) tumour cells (left middle panel and inset; $n = 12$). Beginning on day 18, a few single DsRed$^+$ B16 cells adhere to GFP$^+$ bone marrow clusters (right middle panel), and by day 23, DsRed$^+$ tumour cells proliferate at cluster sites (right panel; $n = 8$). DAPI stain (blue) shows cell nuclei. **c**, A graph showing flow cytometric data of bone marrow-derived GFP$^+$ BMDCs and DsRed$^+$ B16 cells in the lung, and two flow diagrams on day 14 (left panel) and day 18 (right panel) ($n = 30$; error bars show s.e.m.). **d**, GFP$^+$ BMDCs mobilized with B16 conditioned media, then DsRed-tagged tumour cells injected through the tail vein adhere 24 h later (right panel, arrows) compared with animals receiving media alone (left panel; $P < 0.01$). Inset shows proliferating tumour cells in a cluster after four days (right panel inset; $n = 6$). **e**, Number of clusters per ×100 objective field in animals with intradermal LLC or B16

tumours (n = 12). Scale bar on top left panel applies to panels **a** (left, left middle, right middle, 80 μm; left middle inset, 8 μm; right, 20 μm; right inset, 47 μm), **b** (left, left middle, 80 μm; left middle inset, 8 μm; right middle, right, 40 μm) and **d** (40 μm; right inset, 20 μm).

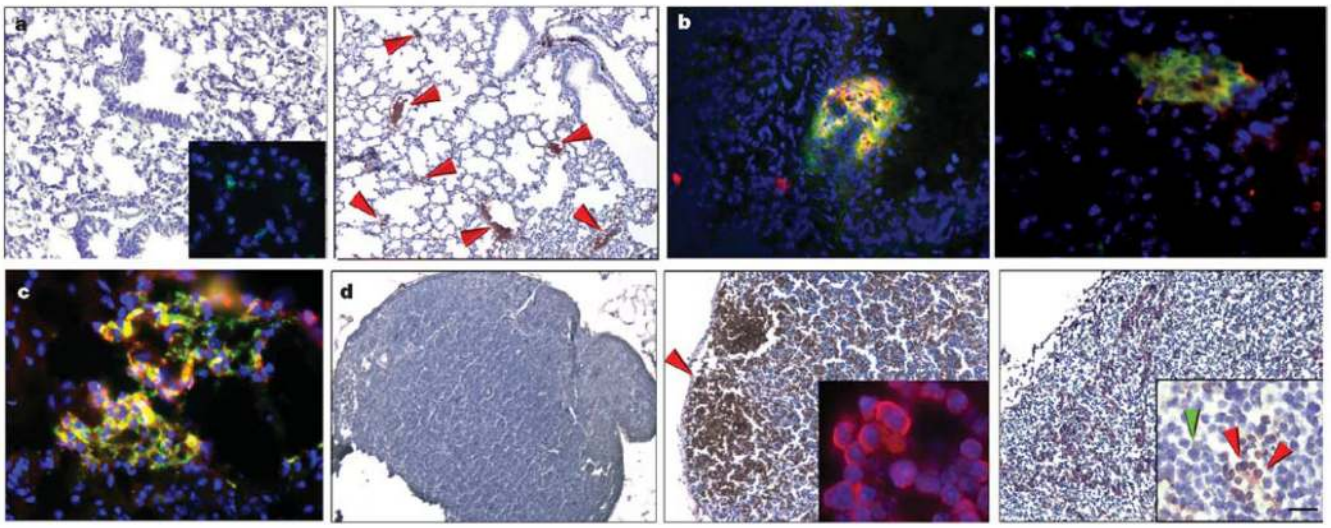

Figure 2. Pre-metastatic clusters are comprised of VEGFR1$^+$ haematopoietic progenitors

a, VEGFR1 staining in irradiated lung before tumour implantation (left panel and inset; n = 10) and 14 days after LLC cell implantation showing clusters in the lung (right panel, arrows; $n = 18$, $3.9 \pm 0.2\%$ cells with VEGFR1 staining per ×100 objective field, $P < 0.05$). **b**, **c**, Double immunofluorescence in the lung of an animal with day 14 LLC tumour. **b**, VEGFR1$^+$ (red) and GFP$^+$ (green) bone marrow cells (left panel), VEGFR1$^+$ (red) and CD133$^+$ (green) (right panel). **c**, VEGFR1$^+$ (red) and CD117$^+$ (green). **d**, VEGFR1$^+$ clusters in c-Myc transgenic lymph node at day 40 of life and before tumorigenesis (middle panel and inset showing VEGFR1$^+$ cells (red)) as compared with wild-type littermate lymph node without the transgene (left panel), and day 120 c-Myc transgenic node with lymphoma (right panel). In the inset of the right panel, arrows indicate the VEGFR1$^+$ clusters (red) surrounded by lymphoma (green) (n = 6). Scale bar at bottom right applies to panels **a** (80 μm; left inset, 40 μm), **b** (20 μm), **c** (20 μm) and **d** (80 μm; insets, 8 μm).

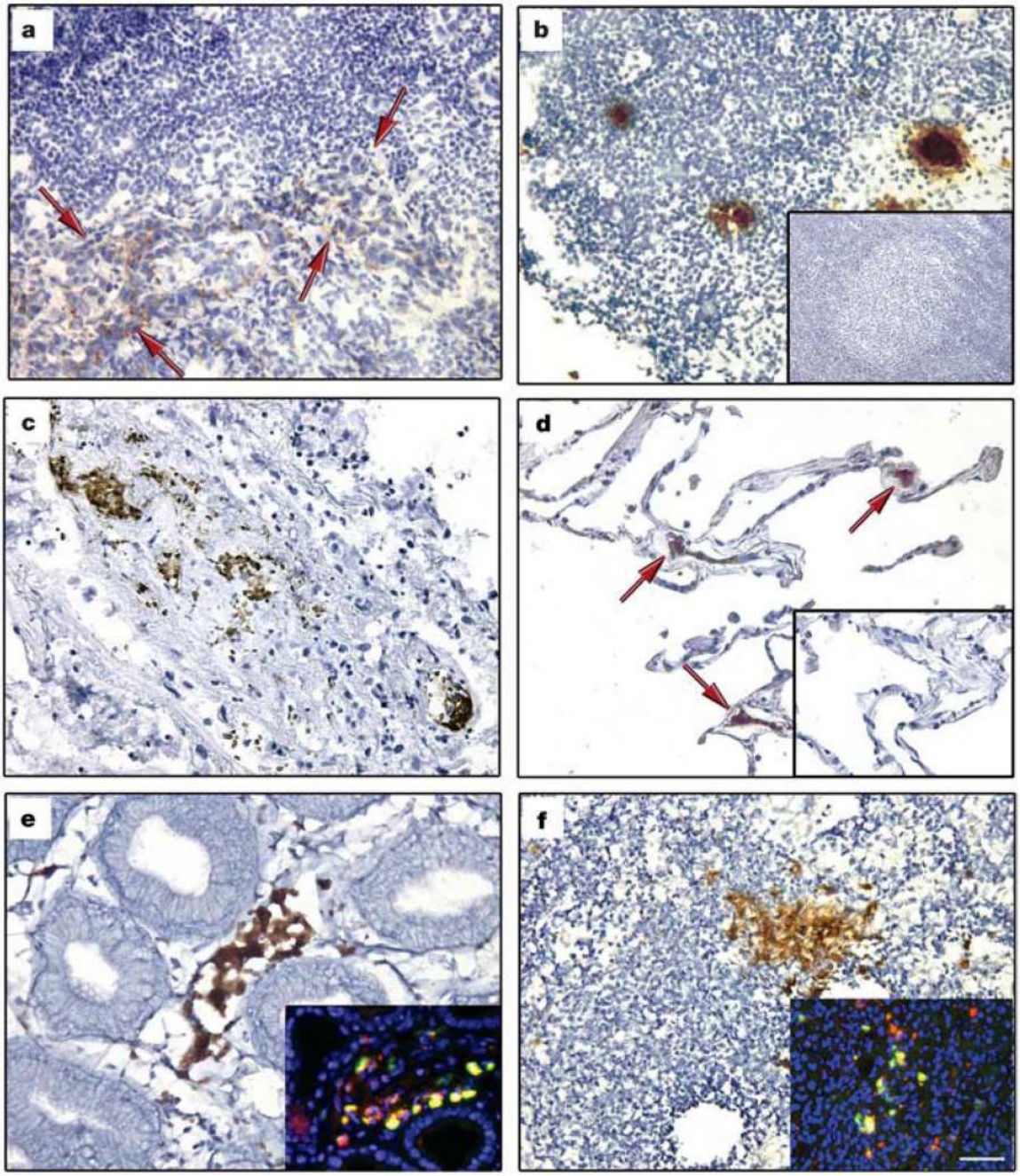

Figure 3. Expression of VEGFR1 in pre-metastatic human tissue

a–f, Cellular clusters stained with VEGFR1 in malignant and non-malignant tissues in individuals with breast ($n = 15$), lung ($n = 15$) and gastrointestinal ($n = 3$) cancers. Lymph node with evidence of breast adenocarcinoma metastasis (**a**, red arrows indicate tumour) and lymph node without malignancy from same patient (**b**). Primary lung adenocarcinoma (**c**) and adjacent 'normal' lung without neoplasm (**d**, red arrows indicate VEGFR1$^+$ cells). No VEGFR1$^+$ clusters were seen in lymph node (**b**, inset; $n = 6$) and lung tissue (**d**, inset; $n = 3$) from individuals without cancer. Also shown is a primary adenosquamous carcinoma of the gastrooesophageal junction (**e**), and a hepatic lymph node without carcinoma (**f**). Insets in **e**,

f, show co-immunofluorescence of VEGFR1 (red) and c-Kit (green). Scale bar at bottom right applies to all panels (40 μm; insets, 40 μm).

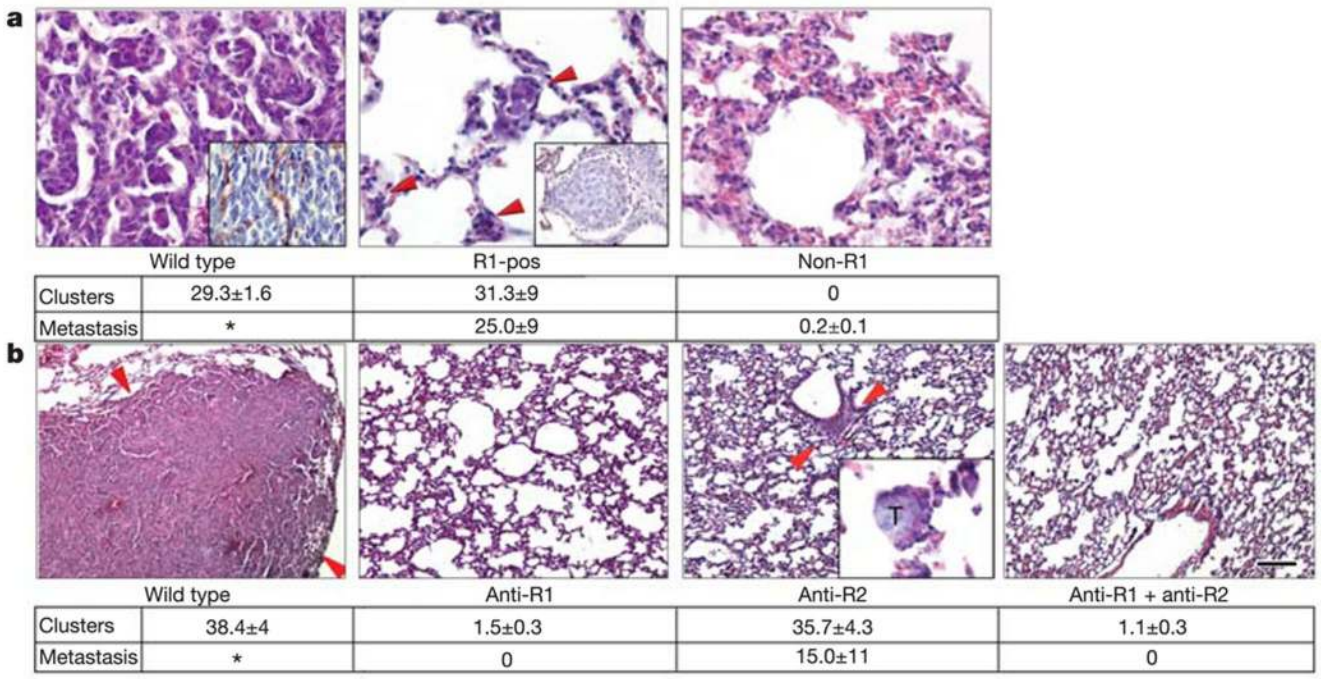

Figure 4. Inhibition of homing of bone marrow cells prevents metastasis

a, VEGFR1$^+$-selected bone marrow (R1-pos) permits micrometastasis (red arrows, middle panel) but prevents well-vascularized large metastases as seen in wild types (left panel), 24 days after LLC implantation. Insets show CD31 (endothelial marker) expression. Bone marrow depleted of VEGFR1$^+$ cells (non-R1) abrogates both clusters and metastases (right panel) ($P < 0.01$ by ANOVA). The table shows the number of clusters and micrometastases per ×100 objective field. *denotes that the metastasis filled the lung. (R1-pos, $n = 4$; non-R1, $n = 4$; wild type, $n = 6$; non-R1 plus wild type, $n = 4$). **b**, Treatment with antibodies to VEGFR1 (anti-R1) and VEGFR2 (anti-R2) in mice with LLC tumours prevents both clusters and metastases ($P < 0.01$ by ANOVA; for all groups, $n = 5$). Arrows in the lung of the wild type denote a large LLC metastasis. Arrows in anti-R2 show a cluster, inset shows a micrometastasis within a cluster. T, tumour cells. The table shows the number of clusters and LLC micrometastases in lung per ×100 objective field. *denotes that the metastasis filled the tissue. Scale bar at bottom right applies to panels **a** (20 μm; wild type inset, 26 μm; R1-pos inset, 32 μm) and **b** (40 μm; anti-R2 inset, 20 μm).

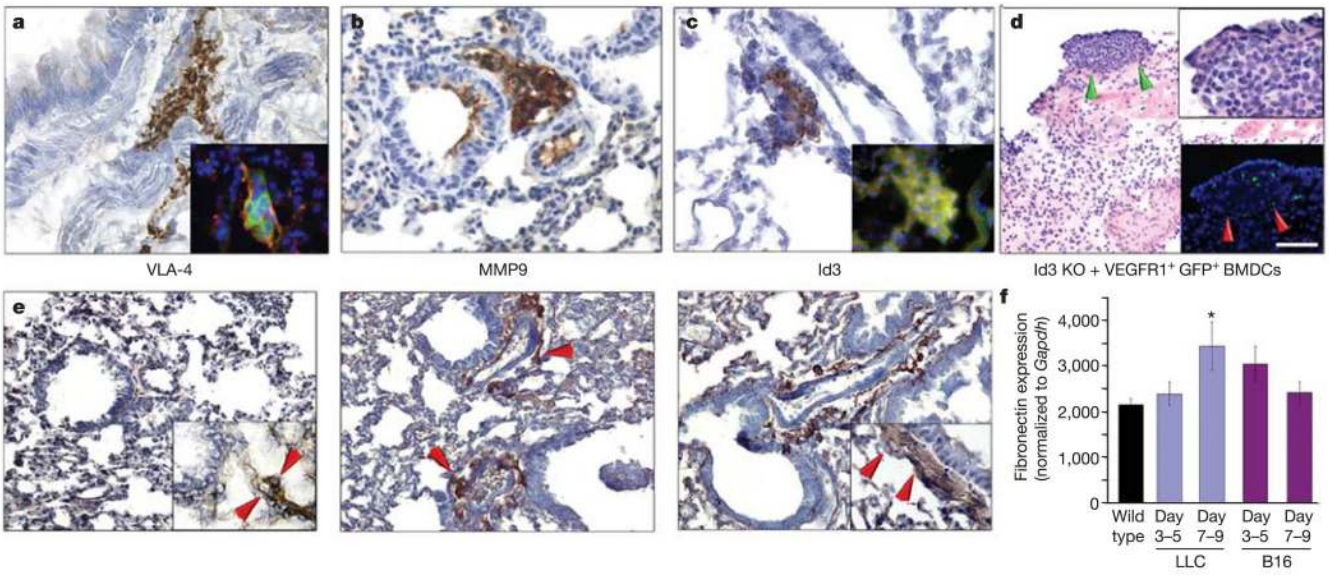

Figure 5. The VLA-4/fibronectin pathway mediates cluster formation

a–c, Wild-type mice 14 days after tumour implantation develop clusters expressing VLA-4 (inset, VEGFR1 (red) and VLA-4 (green)), MMP9 and Id3 (inset, VEGFR1 (red) and Id3 (green)). **d**, Lung tissue in Id3 knockout (KO) mice with LLC tumours given $VEGFR1^{+}GFP^{+}$ BMDCs ($P < 0.01$ by ANOVA; $n = 6$). Green arrows show region in upper inset. Red arrows (lower inset) show the site of metastasis with $GFP^{+}VEGFR1^{+}$ cells. **e**, Baseline fibronectin expression in the wild-type lung ($n = 6$) (left panel). Increased stromal fibronectin in the peribronchial region of the pre-metastatic lung at day three (middle panel, arrows), with maximal expression on day 14 (right panel). Insets, PDGRFα expression indicates resident fibroblasts laying down fibronectin. **f**, Quantitative RT–PCR reveals increased fibronectin expression in the lungs of mice with LLC tumours compared with wild type (*$P < 0.05$ by ANOVA; $n = 6$), and a similar earlier trend in lungs from animals with B16 melanoma. Scale bar at top right applies to panels **a**, **b**, **c** (40 μm; insets, 8 μm), **d** (80 μm; top right inset, 20 μm; bottom right inset 80 μm) and **e** (40 μm; insets, 20 μm).

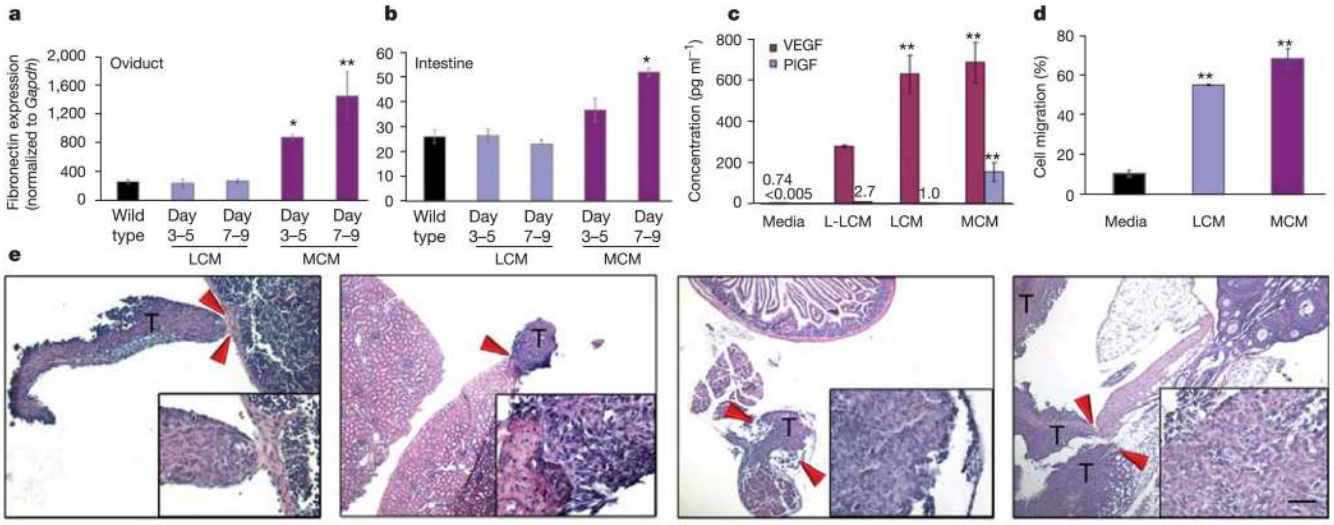

Figure 6. Redirection of LLC metastases to atypical sites

a, **b**, By quantitative RT–PCR analysis, increased fibronectin expression was seen in the oviduct (**a**) and intestine (**b**) in mice given MCM compared with wild-type and LCM-treatment. For oviduct, $*P < 0.05$ at days 3–5 and $**P < 0.001$ for days 7–9 compared with wild type, and for intestine, $*P < 0.001$ at days 7–9 compared with wild type by ANOVA ($n = 6$). **c**, ELISA assay (in triplicate) for VEGF and PlGF levels in the conditioned media ($*P < 0.05$ when compared with L-LCM, $**P < 0.01$ when compared with media alone, by ANOVA). **d**, Transwell migration assays (in triplicate) demonstrate enhanced migration of $VEGFR1^+$ cells to LCM and MCM ($**P < 0.001$ by ANOVA). **e**, Treatment with MCM redirects the metastatic spread of LLC to B16 melanoma metastatic sites, such as the spleen (left panel), kidney (left middle panel), intestine (right middle panel) and oviduct (right panel). Arrows denote the regions of metastatic borders, which are shown in the insets ($n = 6$). T, LLC tumour cells. Scale bar at bottom right applies to panel **e** (200 μm; insets, 20 μm).